A Novel Mach–Zehnder Interferometer Based on Dual-ARROW Structures for Sensing Applications

Shih-Hsin Hsu, *Student Member, IEEE, Student Member, OSA*, and Yang-Tung Huang, *Member, IEEE*

***Abstract*—A novel Mach–Zehnder interferometer (MZI) based on dual antiresonant reflecting optical waveguides (ARROWs) for sensing is proposed. By adjusting the degree of structural symmetry to control the coupling behavior of the dual ARROW, an interferometric sensor without any bending structure can be realized. Operating principles and simulation characteristics of the device are discussed in detail. The refractive-index detection limit of the order of 10^{-5} is achieved.**

***Index Terms*—Integrated optics, interferometry, optical planar waveguides, waveguide couplers.**

I. Introduction

INTEGRATED optical devices have been increasingly used for chemical and/or biochemical sensing applications [1], [2]. These devices feature high sensitivity, miniaturization, mechanical stability, and freedom from electromagnetic interference (EMI). By using the standard silicon-fabrication process, they offer the possibility of fabricating multiple sensors on a single chip for simultaneous detection and the prospect of integrating optical and electrical functions to form smart sensor systems. Among various kinds of transduction (readout) techniques, interferometry is widely adopted due to its inherent higher sensitivity [3]–[5]. Integrated optical interferometers of the Fabry–Pérot and Mach–Zehnder types for chemical and biochemical sensing applications have been realized [6]–[9]. The Mach–Zehnder configuration seems to be the most popular because of its simplicity in design and fabrication and of the presence of the reference arm that is useful for the compensation of the common-mode effect.

In a Mach–Zehnder interferometer (MZI), the incoming coherent light wave is equally split into two channels, and after a certain distance of propagation, the waves from both channels are recombined together. One of the channels [the phase-modulating arm (a.k.a., sensing arm for sensing applications)] is exposed to the outer medium for a certain distance L (interaction length), while the other channel (the reference arm) is isolated from the medium. During this distance, the wave in the phase-modulating arm will experience a phase shift with respect to the wave in the reference arm. At the output port, light coming from both channels will interfere and show a sinusoidal variation corresponding to the accumulated phase difference, which is related to the change of the refractive index of the surrounding medium. An integrated MZI usually comprises two back-to-back splitters/combiners, such as symmetric Y-junctions or directional couplers, connected by a pair of widely separated straight waveguides, as shown in Fig. 1. The wide separation between the two arms requires a lengthy bending structure for the signals to be split into or recombined from the channels, and thus, limits the capability to shrink the device size.

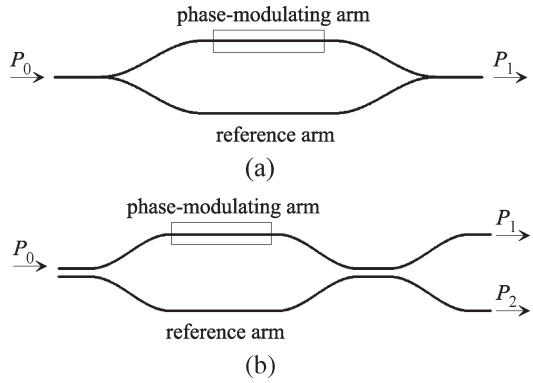

Fig. 1. Configurations of MZIs.

To get relief from this limitation, we propose a novel MZI based on dual antiresonant reflecting optical waveguides (ARROWs) [10]. As a result of the fact that the coupling length of dual-ARROW directional couplers does not increase monotonically with the waveguide separation [11], and the maximum coupling efficiency can be controlled from near 100% to 0% by simply varying the thickness of the outermost cladding layers to adjust its symmetry [12], a compact MZI without any bending structure can be realized. In Section II, we briefly discuss the coupling behavior and the coupling efficiency control of dual-ARROW devices. The configuration and operating principle of the dual-ARROW MZI is given in detail in Section III. To verify the functionality, a design example and the simulation results of the interferometer for chemical sensing are presented in Section IV. Finally, a brief conclusion is provided in Section V.

II. Coupling Behavior of the Dual-Arrow Structure

In contrast to conventional waveguides, ARROW structures utilizing antiresonant reflection as a guiding mechanism instead of total internal reflection can guide waves in low-index cores on a high-index substrate and perform low-loss single-mode

Manuscript received December 24, 2004; revised July 20, 2005. This work was supported by the National Science Council of the Republic of China under Contract NSC92-2215-E-009-048.

The authors are with the Department of Electronics Engineering and Institute of Electronics, National Chiao Tung University, Hsinchu 30010, Taiwan, R.O.C. (e-mail: shhsu@iol.ee.nctu.edu.tw).

Digital Object Identifier 10.1109/JLT.2005.859435

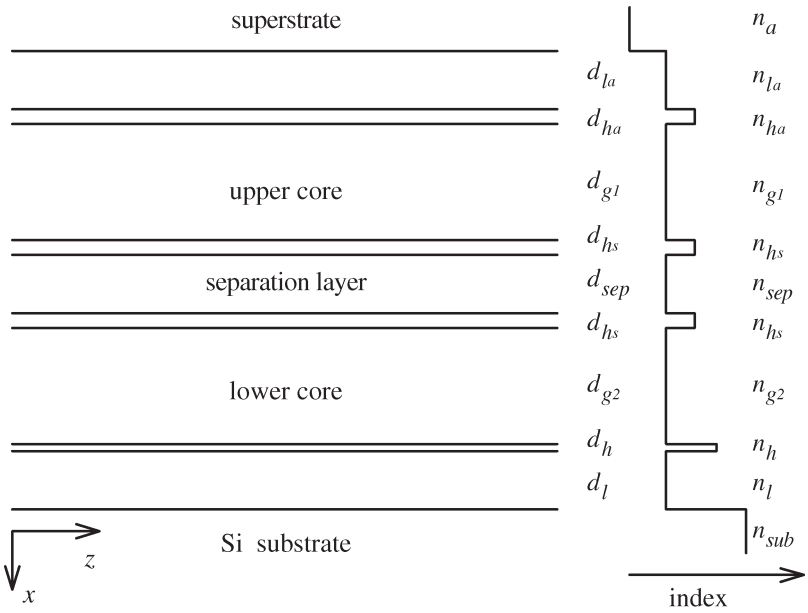

Fig. 2. Schematic view of a dual-ARROW waveguide.

propagation with a relatively large core size to provide efficient coupling with single-mode fibers [10]. With this structure, they are attractive because of many unique features, such as polarization and wavelength-selective behaviors, flexible design rules for the dimensions of core and cladding layers, and relaxed fabrication tolerance. Moreover, the coupling length of ARROW-based couplers does not increase but varies as a periodic function of waveguide separation such that remote coupling can be realized [13]. Based on our previous investigation [12], it is found that a dual ARROW can operate as a directional coupler or two decoupled waveguides by controlling the coupling behavior.

The basic configuration of a dual-ARROW waveguide $(n_{\rm a}/n_{\rm l_a}/n_{\rm h_a}/n_{\rm g_1}/n_{\rm h_s}/n_{\rm sep}/n_{\rm h_s}/n_{\rm g_2}/n_{\rm h}/n_{\rm l}/n_{\rm sub})$, consisting of two parallel ARROW waveguides, is depicted in Fig. 2. The core layers of the two ARROW waveguides are with low refractive indices of $n_{\rm g_1}$ and $n_{\rm g_2}$ and thicknesses of $d_{\rm g_1}$ and $d_{\rm g_2}$, respectively. Between two waveguide cores is a three-layered separation with a high–low–high index profile $n_{\rm h_s}/n_{\rm sep}/n_{\rm h_s}$ and corresponding thicknesses $d_{\rm h_s}/d_{\rm sep}/d_{\rm h_s}$. Interference cladding layers with indices $n_{\rm h}/n_{\rm l}$ and thicknesses $d_{\rm h}/d_{\rm l}$, respectively, are sandwiched between the lower core and the substrate. Atop the upper core are the outermost cladding layers of indices $n_{\rm l_a}/n_{\rm h_a}$ and thicknesses $d_{\rm l_a}/d_{\rm h_a}$. In order to obtain the highest symmetry, the refractive indices and thicknesses of the core layers are set to be the same. Except the outermost cladding layers of thicknesses $d_{\rm l_a}$ and $d_{\rm h_a}$, all cladding layers satisfy the transverse antiresonance condition as [14]

$$d_j \simeq \frac{\lambda_0}{4n_j}\left[1-\left(\frac{n_{\rm g_1}}{n_j}\right)^2+\left(\frac{\lambda_0}{2n_j d_{g,e}}\right)^2\right]^{-\left(\frac{1}{2}\right)}\cdot(2Q_j+1)$$
$$Q_j = 0,1,2,\ldots \quad (1)$$

where $d_{g,e}$ is the effective core thickness and $j = {\rm h_s}$, h, and l, representing corresponding high-index separation, high-index cladding, and low-index cladding layers, respectively.

As for the separation layer, it is worth noting that ARROW-based couplers possess another peculiar character that does not occur in conventional two-channel directional couplers. The thickness of the separation layer could be freely chosen to tailor the coupling length if the coupling structure is used for complete power transfer (i.e., full couplers), as discussed in [11] and [13], but for the case of 3-dB couplers required in this paper, only structures with an antiresonant separation layer can achieve a splitting ratio very close to 50/50. This is because the two-mode coupling condition is best satisfied at antiresonant separations. As the separation approaches resonance, the three-mode coupling effect becomes more and more significant [15] and a more substantial fraction of power will remain in the separation layer at the 3-dB splitting length, and at a resonant separation, the dual-ARROW structure turns out to be impossible to design as a 3-dB coupler. Therefore, the separation layer has to satisfy (1) as well.

The coupling efficiency $C(z)$ from one waveguide core (say, the upper core) to the other (the lower core) at any position z can be defined as the ratio of the power transferred $\Delta P_2(z)$ to the initial power $P_1(0)$, and can be expressed as [12]

$$C(z) \equiv \frac{\Delta P_2(z)}{P_1(0)} = C_0 \sin\left(\frac{\beta_e-\beta_o}{2}z\right) \quad (2)$$

where P_1 and P_2 are the guided powers in the upper and lower cores, and β_e and β_o are the propagation constants of the fundamental even and odd modes, respectively. C_0 represents the maximum coupling efficiency at the coupling length $z = L_0 \equiv \pi/(\beta_e-\beta_o)$. Since the coupling behavior between dual-ARROW waveguides strongly depends on the degree of the structural symmetry, the thickness of the outermost cladding

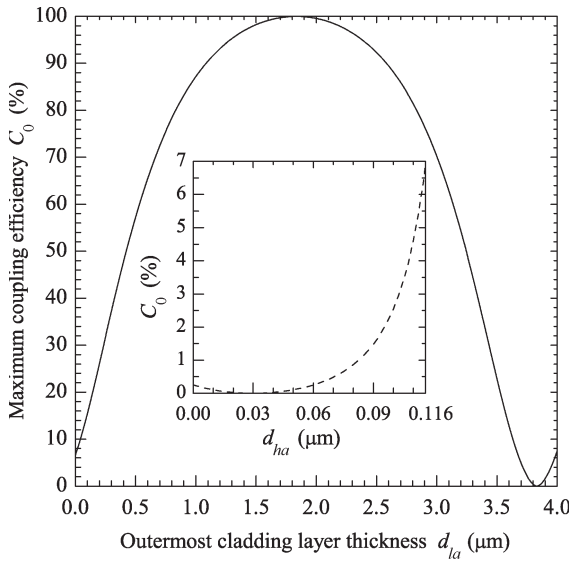

Fig. 3. Maximum coupling efficiency as a function of thickness of the outermost cladding layers. The parameters are $n_{g_1} = n_{g_2} = n_l = n_{sep} = n_{l_a} = 1.46$, $n_h = n_{h_s} = n_{h_a} = 2.00$, $d_{g_1} = d_{g_2} = 4.00$ μm, $d_l = d_{sep} = 2.00\,\mu$m, $d_h = d_{h_s} = d_{h_a} = 0.116\,\mu$m, and $\lambda_0 = 0.6328\,\mu$m. The inset plot shows the dependence on d_{h_a} when $d_{l_a} = 0$.

layers can be adjusted to vary the symmetry degree, and thus, control the coupling efficiency between two waveguides [12]. Fig. 3 shows the dependence of the maximum coupling efficiency on the thickness of the outermost cladding layers d_{l_a} and d_{h_a}. It can be seen that an efficient coupling occurs when the structure possesses relatively high symmetry ($d_{l_a} \simeq 1.83$ μm); the maximum coupling efficiency is close to 100%. When the outermost low-index cladding layer is completely removed ($d_{l_a} = 0$), however, the decoupled phenomenon occurs with the maximum coupling efficiency dropping to less than 10%. In addition, the outermost high-index cladding layer can be partially etched as well to further spoil the structural symmetry, and thus, lower the maximum coupling efficiency to near zero, as shown in the inset of Fig. 3. For instance, the maximum coupling efficiency C_0 can be lowered to less than 0.01%, from about 7% when the thickness d_{h_a} is reduced to 0.030 μm from the antiresonant thickness of 0.116 μm.

III. Configuration and Operating Principle

As illustrated in Fig. 1, an integrated optical MZI typically has two Y-junctions [Fig. 1(a)] or directional couplers [Fig. 1(b)], which act as the splitter or combiner. The waveguides utilized in these interferometers only support a single mode at the operating wavelength λ_0. Light propagating in one arm of the interferometer is affected by the variation of the optical properties of the outer medium (superstrate) during the interaction length L. As a result of a change in the effective index of the waveguide mode Δn_{eff}, the wave will experience a phase shift $\Delta\phi = k_0 \Delta n_{\text{eff}} L$, where $k_0 = 2\pi/\lambda_0$ is the free-space wavenumber. For the interferometer with a combiner of Y-junction type, the waves from the two arms will recombine and couple to radiation modes if they are out of phase. In the case of the directional-coupler type, on the other hand, it is advantageous that the sum of outputs can be used as a reference for the total input power since the power is not lost into radiation. The normalized powers of the two output ports can be expressed as [16]

$$\frac{P_1}{P_0} = \sin^2\left(\frac{\Delta\phi}{2}\right) \tag{3}$$

$$\frac{P_2}{P_0} = \cos^2\left(\frac{\Delta\phi}{2}\right) \tag{4}$$

where P_0 is the input power.

The configuration of the proposed dual-ARROW MZI resembles traditional MZIs with directional-coupler splitters/combiners in slab-waveguide form. Fig. 4 depicts the basic structure of the proposed dual-ARROW MZI that is composed of three sections of dual-ARROW waveguides. The first and third sections are of dual-ARROW structures with the maximum coupling efficiency near 100% and act as 3-dB couplers to split and recombine the light signals, respectively. Therefore, the length of these two sections should be equal to a half of the coupling length of the structure. The second section, whose outermost low-index cladding layer is completely removed, is a decoupled dual-ARROW structure acting as both the phase-modulating and reference arms. The purpose of the partial etching of the outermost high-index cladding layer is twofold. First, as mentioned in the previous section, the maximum coupling efficiency can be further lowered such that the light waves propagating in the reference arm are virtually isolated from the waves in the phase-modulating arm. For sensing applications, a thinner high-index cladding layer can enhance the interaction of waves in the sensing arm with the surrounding medium, and thus, increase the sensitivity.

Assume that a Gaussian beam is launched into either core at the input end of the device. The input-field profile can be expressed as the superposition of all eigenmodes

$$\Psi(x) = \sum_{\nu} c_\nu \psi_\nu(x) \tag{5}$$

where c_ν and $\psi_\nu(x)$ are the field-excitation coefficient and modal field distribution of mode ν, respectively. Based on the modal analysis of the structure, it is found that there are only two low-loss TE modes that are highly excited with excitation efficiencies ($|c_e|^2$ and $|c_o|^2$) greater than 48.5% and will dominate the propagation. The field profiles of the fundamental even (symmetric) and odd (antisymmetric) TE modes in the coupling section are shown in Fig. 5(a). It can be seen that the field distributions are similar to those of the even and odd modes of a typical directional coupler. Other modes existing in the waveguide are either mainly located in the claddings or too lossy to be significant. Besides, the excitation efficiencies of these modes are all lower than 0.8%. If the Gaussian input is launched into the upper core, the input field distribution will be mainly concentrated in the upper core and can be approximately represented as the superposition of the two dominant modes, as shown in Fig. 5(b). The output after the propagation of a coupling length will primarily locate in the lower core, as

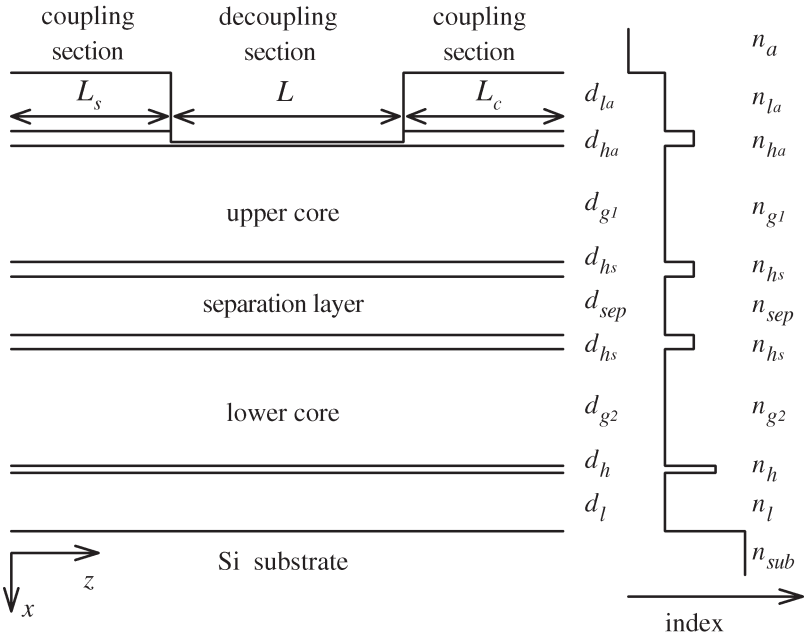

Fig. 4. Schematic view of the dual-ARROW MZI.

depicted in the dotted curve of Fig. 5(b). Now that the length of the coupling section is set to be equal to a half of the coupling length, the coupling section can function as a 3-dB coupler.

For the decoupling section, the field profiles of the two dominant TE modes are shown in Fig. 6. It is obvious that light waves of the two modes are predominantly confined in individual channels. The wave residing in the sensing arm (the upper core) interacts with the outer medium and is substantially influenced by the variation of the medium. Meanwhile, the wave in the reference arm (the lower core) is almost unaffected, due to its extremely low evanescent-wave portion. After a certain distance of propagation, the recombined light waves interfere and the output powers provide the required information to extract the phase shift $\Delta\phi$ obtained, and thus, the change of the refractive index of the surrounding medium $\Delta n_{\rm a}$.

IV. Design Example and Simulation Results

In this section, an MZI sensor based on the dual-ARROW structure is used as a design example. The design example is based on a silicon substrate ($n_{\rm sub} = 3.85$ at the operating wavelength $\lambda_0 = 0.6328$ μm) in an aqueous environment ($n_{\rm a} = 1.332$). Silicon dioxide (SiO_2) with a refractive index of 1.46 is used for the upper and lower cores ($n_{\rm g_1}$ and $n_{\rm g_2}$), the separation layer ($n_{\rm sep}$), and the low-index cladding layers ($n_{\rm l}$ and $n_{\rm l_a}$). Silicon nitride (Si_3N_4) is adopted as the high-index cladding near the substrate to maintain low propagation loss, i.e., $n_{\rm h} = 2.00$. Since the refractive index of other high-index cladding layers either determines the coupling length of the coupling section and the degree of virtual isolation in the sensing section ($n_{\rm h_s}$), or affects the amount of the evanescent-field penetration and the sensitivity in the sensing section ($n_{\rm h_a}$), silicon oxynitride (SiON) with a refractive index ranging from 1.46 (SiO_2) to 2.00 (Si_3N_4) is employed [17], and the suitable values will be discussed later. The thicknesses $d_{\rm g_1}$ and $d_{\rm g_2}$ of

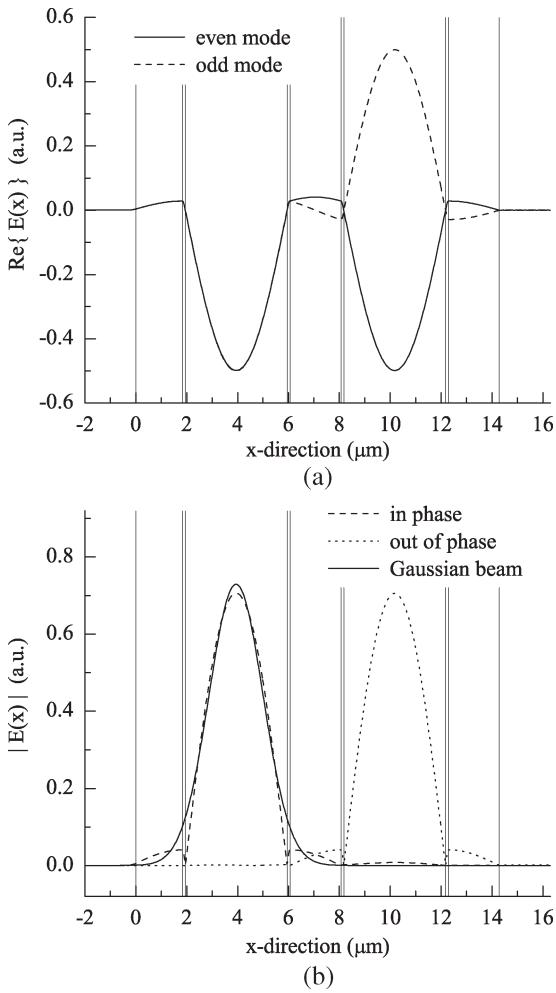

Fig. 5. Field profiles of (a) the fundamental even and odd TE modes in the coupling section with $n_{\rm g_1} = n_{\rm g_2} = n_{\rm l} = n_{\rm sep} = n_{\rm l_a} = 1.46$, $n_{\rm h} = n_{\rm h_s} = n_{\rm h_a} = 2.00$, $d_{\rm g_1} = d_{\rm g_2} = 4.00$ μm, $d_{\rm l} = d_{\rm sep} = 2.00$ μm, $d_{\rm h} = d_{\rm h_s} = d_{\rm h_a} = 0.116$ μm, $d_{\rm l_a} = 1.83$ μm; (b) the superposition of these two modes with 0 (dashed curve) and π (dotted curve) phase differences and the input Gaussian beam (solid curve).

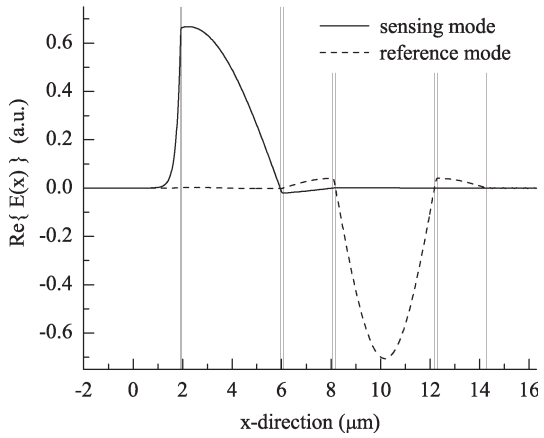

Fig. 6. Field profiles of the two dominant TE modes in the decoupling section with $d_{\mathrm{h_a}} = 0.030$ μm, $d_{\mathrm{l_a}} = 0$ μm, and all others are the same as in Fig. 5.

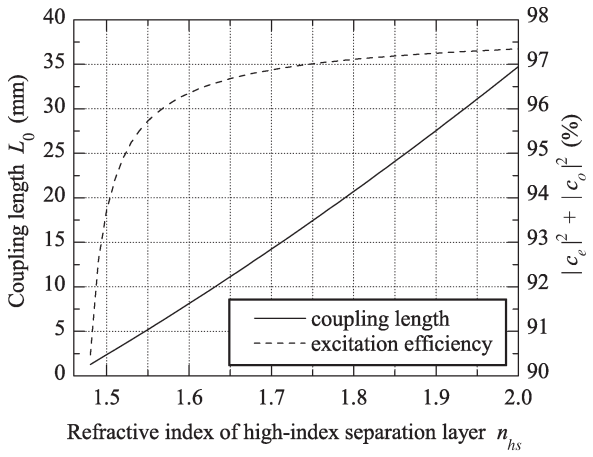

Fig. 7. Dependence of the coupling length L_0 (solid line) and combined excitation efficiency $|c_e|^2 + |c_o|^2$ (dashed curve) of the two dominant TE modes of the coupling section on the refractive index of the high-index separation layer $n_{\mathrm{h_s}}$. The parameters are the same as in Fig. 5, except $n_{\mathrm{h_s}}$ and the corresponding $d_{\mathrm{h_s}}$.

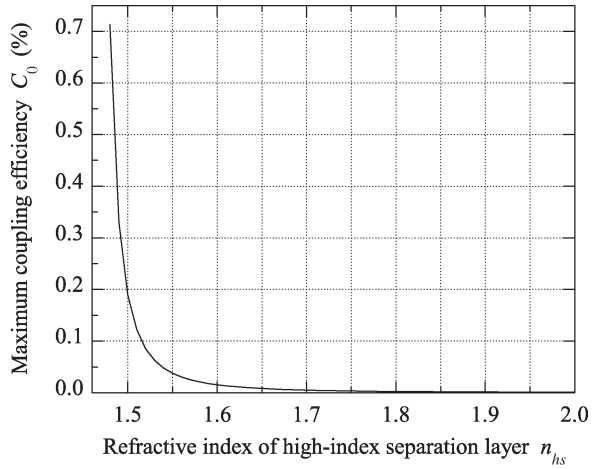

Fig. 8. Maximum coupling efficiency of the sensing section. The parameters are the same as in Fig. 6, except $n_{\mathrm{h_s}}$ and $d_{\mathrm{h_s}}$.

the waveguide cores are chosen to be 4.00 μm, the thickness of the separation is 2.00 μm, and the thicknesses of the other layers, except $d_{\mathrm{h_a}}$ and $d_{\mathrm{l_a}}$, are determined according to (1).

As a result of the fact that the outermost high-index cladding layer can cause the field distribution of the sensing mode to shift toward the outer medium and enhance the interaction between the medium and the sensing wave, as depicted in Fig. 6, a higher value of the refractive index $n_{\mathrm{h_a}}$ is desired. To make the design simple and sensitive to the refractive-index variation of the surrounding medium, $n_{\mathrm{h_a}} = n_{\mathrm{h}} = 2.00$ is used. As for the refractive index of the high-index separation layer $n_{\mathrm{h_s}}$, the dependence of the coupling length of the coupling section on $n_{\mathrm{h_s}}$ is displayed in Fig. 7 (solid line). It can be seen that the coupling length is approximately proportional to the index $n_{\mathrm{h_s}}$. To have a device of small size, a lower value of $n_{\mathrm{h_s}}$ is preferred. However, the combined excitation efficiency of the two dominant modes $|c_e|^2 + |c_o|^2$ (the dashed curve in Fig. 7) will become lower and contributions from other modes (cladding and higher order modes) in wave propagation along the coupling sections will increase if a lower value of $n_{\mathrm{h_s}}$ is used. Moreover, a lower refractive index of the high-index separation layers may not provide the required isolation between the sensing mode (arm) and the reference mode (arm) in the sensing section. Fig. 8 shows the maximum coupling efficiency for the sensing section versus the refractive index of the high-index separation layers. To minimize the power transfer between two arms in the sensing section, a value of $n_{\mathrm{h_s}}$ which is not too low is required. Hence, $n_{\mathrm{h_s}} = 1.60$ is adopted in the following examples.

As discussed in the previous section, the thickness of the outermost cladding layers $d_{\mathrm{h_a}}$ and $d_{\mathrm{l_a}}$ determines the coupling behavior of the dual-ARROW structure. Therefore, they are chosen to be $d_{\mathrm{h_a}} = 0.116$ μm and $d_{\mathrm{l_a}} = 1.83$ μm to have a maximum coupling efficiency near 100% in the coupling section. While in the sensing section, $d_{\mathrm{l_a}}$ is zero, and $d_{\mathrm{h_a}} = 0.030$ μm is used to achieve an extremely low coupling efficiency and high sensitivity. Table I summarizes the structural parameters of the dual-ARROW MZI sensor.

With the aforementioned structure and throughout the interested superstrate-index variation ranging from $n_{\mathrm{a}} = 1.330$ to 1.360, the coupling length of the coupling section is found to be 8.12 mm, and then, the lengths of the first and third sections are both a half of it for acting as 3-dB couplers, i.e., $L_{\mathrm{s}} = L_{\mathrm{c}} = 4.06$ mm. The total length of the device will now be $(L + 8.12)$ mm. The propagation losses of the two dominant TE modes are both lower than 0.05 dB/cm in the coupling section and lower than 0.002 (sensing mode) and 0.09 dB/cm (reference mode) in the sensing section. The maximum coupling efficiency is higher than 99.99% in the coupling sections, while in the sensing (decoupling) section, it is lower than 0.1% throughout the range. These results indicate that the coupling and decoupling properties can be maintained in corresponding sections.

The devices with different interaction lengths L are simulated by eigenmode-propagation analysis. Fig. 9 shows the normalized output powers P_1 and P_2 against the superstrate index for the sensor with $L = 5$ mm, and the sum $P_1 + P_2$ is shown as a reference. Due to the leaky nature of ARROW structures, it is expected that the sum of the output powers will be slightly lower than the input power. The main reason for the sum far below unity around $n_{\mathrm{a}} = 1.347$, 1.353, and 1.357 is

TABLE I
STRUCTURAL PARAMETERS OF THE DUAL-ARROW MACH–ZEHNDER-INTERFEROMETER SENSOR

Refractive index		Thickness (μm)	
$n_{g1},\ n_{g2}$	1.46	$d_{g1},\ d_{g2}$	4.00
$n_l,\ n_{sep}$	1.46	$d_l,\ d_{sep}$	2.00
n_{l_a}	1.46	d_{l_a}	1.83 †; 0 ‡
n_h	2.00	d_h	0.116
n_{h_s}	1.60	d_{h_s}	0.240
n_{h_a}	2.00	d_{h_a}	0.116 †; 0.030 ‡

† in the coupling section; ‡ in the decoupling section.

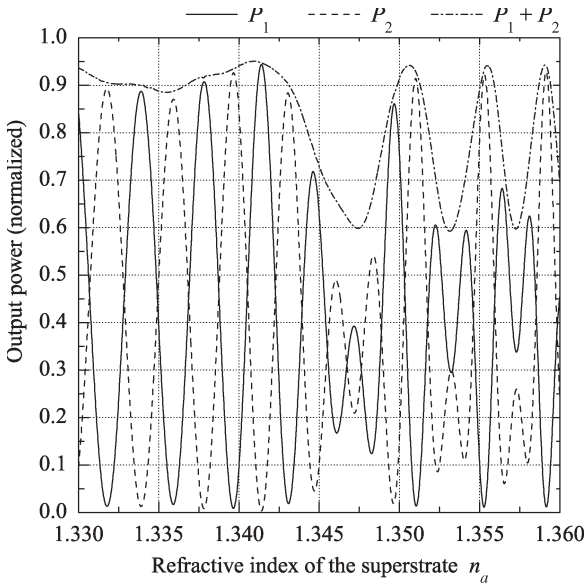

Fig. 9. Output powers P_1, P_2, and $P_1 + P_2$ of the sensor versus the superstrate index. The structural parameters are summarized in Table I, $L_s = L_c = 4.06$ mm, and the interaction length L is 5 mm.

that some of the power couples to highly lossy modes, whose propagation losses are greater than 30 dB/cm, and radiation modes at the abrupt discontinuity between the second and third sections.

Fig. 10 shows the phase change as a function of the refractive index of the outer medium for different structures, and the slope of the curve $\Delta\Phi/\Delta n_a$ can be defined as the sensitivity. For the sensor with the structure described above and an interaction length $L = 15$ mm (a device length of 23.12 mm), the sensitivity obtained is about $676 \cdot (2\pi)$ at $n_a = 1.332$, which corresponds to a minimum detectable refractive-index variation of $\Delta n_{a,min} = 1.48 \times 10^{-5}$ if the phase resolution is $0.01 \cdot (2\pi)$. Another measure of the sensitivity is the rate of change of the modal effective index to the variation of the superstrate index $\Delta n_{eff}/\Delta n_a$ [9], which is 2.85×10^{-2}. The sensitivity of ARROW-based MZI sensors is generally limited due to the good confinement of the guided waves within the core, an intrinsic characteristics of ARROW devices [5]. To increase the sensitivity, a thinner waveguide core is helpful

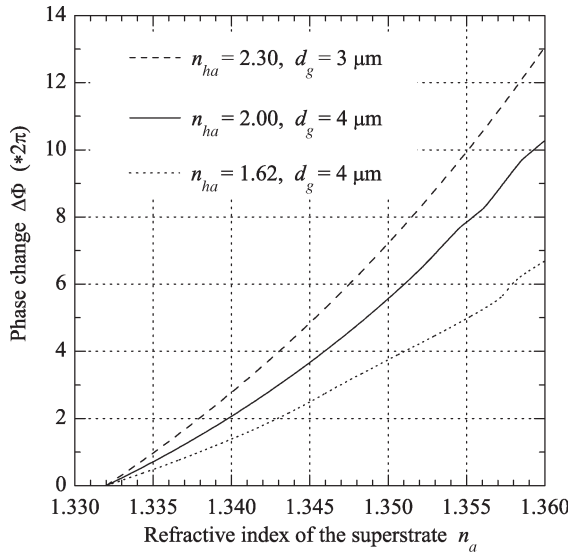

Fig. 10. Phase change as a function of the refractive index of the outer medium for several designs. The interaction length is 5 mm.

since it can reduce the confinement with the penalty of higher propagation loss. By employing a high-index cladding near the substrate with a higher refractive index, this increased loss can be relieved. Another way is to replace the outermost high-index cladding layer with a material of a higher refractive index, which can build up the evanescent wave, and thus, enhance the interaction between the superstrate and the sensing wave. For instance, the value of $\Delta n_{eff}/\Delta n_a$ for the device with $d_g = 3.00$ μm and $n_{h_a} = 2.30$ (dashed line in Fig. 10) can be increased to 3.94×10^{-2}. The detection limit of the superstrate-index variation can be lowered to $\Delta n_{a,min} = 1.07 \times 10^{-5}$ with an interaction length of 15 mm and a device size of 17.61 mm.

In comparison, Heideman *et al.* [8] have reported a slab waveguide MZI sensor with an index-detection limit of about 4×10^{-6}, but the whole interferometric setup is somewhat bulky. Schipper *et al.* [3] proposed a more integrated MZI sensor with higher sensitivity, however, the tiny dimensions of the waveguide structure makes it difficult to reliably fabricate and efficiently couple with fibers. The first rib-ARROW-based MZI sensor, demonstrated in [5], has a minimum detectable index variation of 2×10^{-5} in a 35-mm device length. The analysis shows that the proposed dual-ARROW MZI sensor, with a smaller device size, can have a higher sensitivity than the rib-ARROW MZI sensor. Although the sensitivity of the proposed device might not be easily competitive to conventional ones, the compact structure and the potential to further shrink the device size are still attractive.

V. CONCLUSION

In this paper, we have proposed and described the operation of a novel Mach–Zehnder interferometer (MZI) based on dual antiresonant reflecting optical waveguide (ARROW) structures. By simply varying the thickness of the outermost cladding layers to control the coupling behavior of the structure, a compact interferometer without any lengthy bends can be fulfilled. To verify its functionality, chemical sensors for use in an aqueous

environment are designed and analyzed. Techniques to improve the sensitivity are also discussed. Within a device length of 24 mm, a refractive-index detection limit of 10^{-5} can be achieved if the phase resolution is $0.01 \cdot (2\pi)$.

ACKNOWLEDGMENT

The authors would like to thank the reviewers for their valuable comments and helpful suggestions.

REFERENCES

[1] P. V. Lambeck, "Integrated opto-chemical sensors," *Sens. Actuators B, Chem.*, vol. 8, no. 1, pp. 103–116, Apr. 1992.

[2] B. J. Luff, R. D. Harris, J. S. Wilkinson, R. Wilson, and D. J. Schiffrin, "Integrated-optical directional coupler biosensor," *Opt. Lett.*, vol. 21, no. 8, pp. 618–620, Apr. 1996.

[3] E. F. Schipper, A. M. Brugman, C. Domínguez, L. M. Lechuga, R. P. H. Kooyman, and J. Greve, "The realization of an integrated Mach–Zehnder waveguide immunosensor in silicon technology," *Sens. Actuators B, Chem.*, vol. 40, no. 2–3, pp. 147–153, May 1997.

[4] B. J. Luff, J. S. Wilkinson, J. Piehler, U. Hollenbach, J. Ingenhoff, and N. Fabricius, "Integrated optical Mach–Zehnder biosensors," *J. Lightw. Technol.*, vol. 16, no. 4, pp. 583–592, Apr. 1998.

[5] F. Prieto, B. Sepúlveda, A. Calle, A. Llobera, C. Domínguez, and L. M. Lechuga, "Integrated Mach–Zehnder interferometer based on ARROW structures for biosensor applications," *Sens. Actuators B, Chem.*, vol. 92, no. 1–2, pp. 151–158, Jul. 2003.

[6] N. Fabricius, G. Gauglitz, and J. Ingenhoff, "A gas sensor based on an integrated optical Mach–Zehnder interferometer," *Sens. Actuators B, Chem.*, vol. 7, no. 1–3, pp. 672–676, Mar. 1992.

[7] A. Brandenburg, R. Edelhäuser, and F. Hutter, "Integrated optical gas sensors using organically modified silicates as sensitive films," *Sens. Actuators B, Chem.*, vol. 11, no. 1–3, pp. 361–374, Mar. 1993.

[8] R. G. Heideman, R. P. H. Kooyman, and J. Greve, "Performance of a highly sensitive optical waveguide Mach–Zehnder interferometer immunosensor," *Sens. Actuators B, Chem.*, vol. 10, no. 3, pp. 209–217, Feb. 1993.

[9] R. G. Heideman and P. V. Lambeck, "Remote opto-chemical sensing with extreme sensitivity: Design, fabrication and performance of a pigtailed integrated optical phase-modulated Mach–Zehnder interferometer system," *Sens. Actuators B, Chem.*, vol. 61, no. 1–3, pp. 100–127, Dec. 1999.

[10] M. A. Duguay, Y. Kokubun, T. L. Koch, and L. Pfeiffer, "Antiresonant reflecting optical waveguides in SiO_2–Si multilayer structures," *Appl. Phys. Lett.*, vol. 49, no. 1, pp. 13–15, Jan. 1986.

[11] M. Mann, U. Trutschel, C. Wachter, L. Leine, and F. Lederer, "Directional coupler based on antiresonant reflecting optical waveguides," *Opt. Lett.*, vol. 16, no. 11, pp. 805–807, Jun. 1991.

[12] Y.-H. Chen and Y.-T. Huang, "Coupling efficiency analysis and control of dual antiresonant reflecting optical waveguides," *J. Lightw. Technol.*, vol. 14, no. 6, pp. 1507–1513, Jun. 1996.

[13] J. Gehler, A. Bräuer, and W. Karthe, "Remote coupling over 93 μm using ARROW waveguides in strip configuration," *Electron. Lett.*, vol. 30, no. 3, pp. 218–220, Feb. 1994.

[14] T. Baba and Y. Kokubun, "Dispersion and radiation loss characteristics of antiresonant reflecting optical waveguides—Numerical results and analytical expressions," *IEEE J. Quantum Electron.*, vol. 28, no. 7, pp. 1689–1700, Jul. 1992.

[15] R. Muschall, F. Lederer, and U. Trutschel, "New ARROW couplers and switches with significantly reduced coupled length," *Int. J. Optoelectron.*, vol. 8, no. 5–6, pp. 537–546, 1993.

[16] B. H. Verbeek, C. H. Henry, N. A. Olsson, K. J. Orlowsky, R. F. Kazarinov, and B. H. Johnson, "Integrated four-channel Mach–Zehnder multi/demultiplexer fabricated with phosphorous doped SiO_2 waveguides on Si," *J. Lightw. Technol*, vol. 6, no. 6, pp. 1011–1015, Jun. 1988.

[17] K. Wörhoff, P. V. Lambeck, and A. Driessen, "Design, tolerance analysis, and fabrication of silicon oxynitride based planar optical waveguides for communication devices," *J. Lightw. Technol.*, vol. 17, no. 8, pp. 1401–1407, Aug. 1999.

Shih-Hsin Hsu (S'99) received the B.S. degree in physics from National Taiwan University, Taipei, Taiwan, R.O.C., in 1994. He is currently working towards the Ph.D. degree in electronics at National Chiao Tung University, Hsinchu, Taiwan.

He has focused his research on integrated optical devices for optical communication and sensing applications.

Yang-Tung Huang (M'90) was born in Taiwan, R.O.C., in 1955. He received the B.S. degree in electrophysics and the M.S. degree in electronics from National Chiao Tung University, Hsinchu, Taiwan, in 1978 and 1982, respectively, and the Ph.D. degree in electrical and computer engineering from the University of Arizona, Tucson, in 1990.

He is a Professor at the Department of Electronics Engineering and the Institute of Electronics, National Chiao Tung University, and has been the Director of the Nano Facility Center since 2003. He has been the Director of the Institute of Electronics for three years, and the Director of Semiconductor Research Center for two years. His current researches include integrated optics, photonic crystal waveguides, biooptoelectronics, and optoelectronic switching networks.

Dr. Huang received the Outstanding Research Award from the National Science Council in 1998.